A Mullins softening criterion for general loading conditions

Yannick Merckel [a], Mathias Brieu [a,*], Julie Diani [b], Julien Caillard [c]

[a] LML, Ecole Centrale de Lille, bd Paul Langevin, 59650 Villeneuve d'Ascq, France
[b] Laboratoire PIMM, CNRS, Arts et Métiers ParisTech, 151 bd de l'Hôpital, 75013 Paris, France
[c] Manufacture Française des Pneumatiques Michelin, CERL, Ladoux, 63040 Clermont-Ferrand, France

A B S T R A C T

Samples of carbon-black filled styrene butadiene rubbers (SBRs) were submitted to successive nonproportional loadings in order to define a general criterion for the Mullins softening. For this purpose, each sample was initially submitted to uniaxial or biaxial preloadings followed by a cyclic uniaxial tension test. An original experimental analysis aimed at defining the activation threshold for the Mullins softening during cyclic uniaxial loadings. The experimental data provide substantial evidences establishing the surface of the maximum directional stretch undergone by the material as a relevant Mullins softening criterion. The latter was used to successfully predict the Mullins softening surfaces for additional loading cases.

Keywords:
Rubber material
Anisotropic material
Mechanical testing
Mullins softening

1. Introduction

Carbon-black filled rubbers exhibit substantial softening when stretched for the first time. This phenomenon is generally referred to as the Mullins softening for the amount of work dedicated to the topic by Mullins (1947, 1949, 1950, 1969). Despite numerous contributions on the Mullins softening over the past decades, no general agreement has been found yet on the activation criterion of this phenomenon for general loading conditions. The objective of this contribution is to provide such a criterion essential for filled rubber constitutive modeling.

The Mullins softening may be illustrated by the stress–stretch response of a filled rubber submitted to a cyclic uniaxial tensile test with increasing maximum stretch. Fig. 1a highlights the stress-softening undergone by a filled rubber when first loaded. One may notice that once the Mullins softening is evacuated, the material behavior evolves very slowly. To the contrary, when stretching the material beyond the maximum intensity previously applied, it softens substantially. One may notice also that while the material softens some residual stretch appears and increases with the maximum stretch applied. Mullins (1947, 1949) conducted extensive experimental studies showing the dependence of filled rubbers softening and residual stretch with the maximum stretch for uniaxial tension tests. The same author revealed the anisotropy of both the Mullins softening and the residual stretch by applying successive nonproportional loadings (i.e. successive loadings, changing the directions of stretching). Subsequent experimental studies focused mainly on proportional loadings, and only a few authors (Laraba-Abbes et al., 2003; Hanson et al., 2005; Diani et al., 2006a,b; Itskov et al., 2006; Dargazany and Itskov, 2009; Machado, 2011) conducted nonproportional loadings showing the anisotropy induced by a preloading when applying a series of loadings according to various directions on the same sample.

* Corresponding author. Tel.: +33 3 20 33 53 75; fax: +33 3 20 33 54 99.
E-mail addresses: yannick.merckel@gmail.com (Y. Merckel), mathias.brieu@ec-lille.fr (M. Brieu), julie.diani@ensam.eu (J. Diani), julien.caillard@fr.michelin.com (J. Caillard).

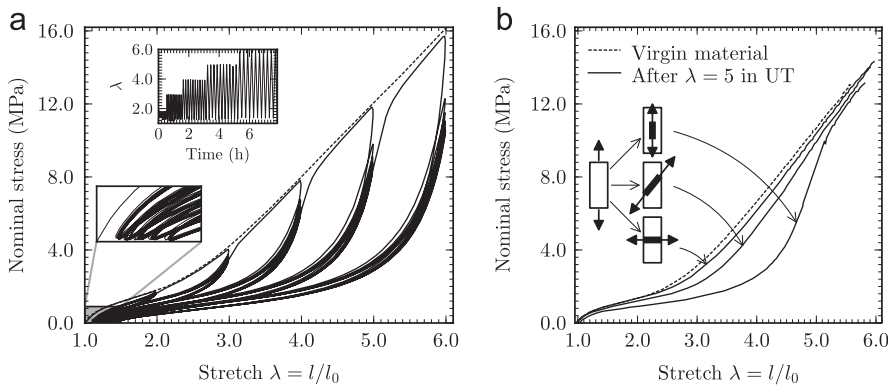

Fig. 1. Mullins softening: (a) Stress–stretch response of a filled rubber under cyclic uniaxial conditions. (b) Evidence of uniaxial tension (UT) preloading induced anisotropy.

At room temperature, the Mullins softening is generally considered as an irreversible damage and therefore is modeled by damage parameters and their evolutions (see Diani et al., 2009 for a review). Most models use an isotropic damage definition for which the damage criterion may be defined in terms of the highest eigenvalue of the deformation gradient tensor (Govindjee and Simo, 1991, 1992), or of the maximum of any deformation tensor invariant (Lion, 1996; Krishnaswamy and Beatty, 2000; Chagnon et al., 2004; Elías-Zúñiga, 2005), or of the maximum free energy (Simo, 1987; Ogden and Roxburgh, 1999), or of other scalar quantities. This idealized isotropic representation of the Mullins softening does not account for the anisotropy induced by the Mullins softening. Actually, very few models deal with an anisotropic criterion. One may cite Göktepe and Miehe (2005) accounting for directional damage parameters depending on the maximum directional free energy, Diani et al. (2006a,b) and Dargazany and Itskov (2009) considering directional maximum stretches as directional criterion of damage activation, and Itskov et al. (2010) using the maximum stretches in the principal directions of the current deformation gradient tensor only. In what follows, an original analysis of nonproportional loading tests provides experimental evidences that the maximum directional stretch surface defines a relevant three-dimensional criterion for the Mullins softening activation.

This paper is organized as follows. The next section presents the experimental setup and describes the original method used to detect the Mullins softening activation. This section also provides the experimental results obtained under nonproportional loading conditions. In Section 3, the Mullins softening criterion is defined and validated for additional loading cases. Finally, concluding remarks close the paper.

2. Experimental determination of the Mullins softening activation

2.1. Experimental setup

For this study, we used a 40 phr carbon-black filled styrene butadiene rubber (SBR) processed by Michelin into final plates of 2.5 mm thickness. The material in-plane isotropy was verified by punching dumbbell samples in various directions in the plates and testing them in uniaxial tension. In order to submit the material to uniaxial and biaxial loading conditions, two testing machines were used. The uniaxial tension tests were conducted on an Instron 5882 uniaxial testing machine at a constant crosshead speed which was chosen in order to reach an average strain rate close to 10^{-2} s^{-1}. Biaxial tests were carried out on a planar biaxial testing device built with four perpendicular electromechanical actuators controlled independently. Any biaxial test is characterized by the biaxial ratio R

$$R = \frac{F_{22}-1}{F_{11}-1} \tag{1}$$

with F_{11} and F_{22} being the longitudinal and transverse stretchings, respectively. Biaxial tension conditions were set such that $F_{11} \geq F_{22}$ and R ranging from 0 (pure shear) to 1 (equi-biaxial tension). All biaxial tests were run at constant crosshead speed corresponding to an average strain rate close to 10^{-2} s^{-1} in the direction 1. For proportional uniaxial tension tests, dumbbell samples of dimension 30 mm long and 4 mm wide were used. For biaxial preloading tests, cross-shaped samples were used. For uniaxial preloadings, large dumbbell specimens, 25 mm wide and 60 mm long, were used. Finally, for cyclic uniaxial tension tests 4 mm wide and 10 mm long dumbbell samples were punched in biaxially or uniaxially preloaded specimens. Strains are measured locally by video extensometry for both machines. Uniaxial tensile test resulting stress is defined by $\sigma = F\lambda/S_0$ with F being the force, $\lambda = l/l_0$ being the stretching, and S_0 being the initial sample cross-section. Let us note that σ denotes the Cauchy stress when incompressibility is assumed, which is common for filled rubbers. Biaxial tests were used for preloadings only, and forces were not recorded for these tests. During subsequent cyclic loadings, the tensile stretch is measured using two paint marks and is defined as $\lambda = l/l_0$, with l_0 being the initial distance between the paint marks for the material virgin of any loading.

At this point, let us clarify some notations that will be used along the study, biaxial preloadings are characterized by the ratio R and the maximum value of stretching is denoted as F_{11}, uniaxial preloadings are characterized by the applied

maximum pre-stretch λ_{pre} and each cycle of the subsequent cyclic uniaxial tension loadings is characterized by the maximum stretch λ_{max} reached during the latter.

2.2. Definition of a parameter for the Mullins softening activation

During a cyclic loading, the material exhibits a significant hysteresis when loaded above the maximum stretch yet undergone. When loaded below the maximum stretch λ_{max}, the material shows fairly close loading and unloading responses. Therefore, any of these responses may be used to characterize its softened behavior, and the loading responses were privileged in the sequel. Along with Mullins softening materials show substantial residual stretch increasing with the applied maximum stretch (Fig. 1a). Therefore, one may want to use the increase in residual stretch as a Mullins threshold activation. Unfortunately, as evidenced by Mullins (1949) and Diani et al. (2006a) the residual stretch is perturbed by the filled rubber viscoelasticity and shows a rapid partial recovery when samples are unclamped. In order to limit interferences between the residual stretch and the material softening, it seems better to correct the actual measured stretch λ according to

$$\lambda^{cor} = \frac{\lambda}{\lambda_{res}}, \tag{2}$$

which withdraws the residual stretch contribution in the cyclic uniaxial tension stress–stretch responses. In order to illustrate the benefit of such a correction, the cyclic loading responses of a uniaxial sample already pre-stretched to $\lambda_{pre} = 2.5$ are plotted in terms of stress vs. amended stretch, λ^{cor}, in Fig. 2a. One notes that the loading responses coincide as long as the Mullins effect is not re-activated ($\lambda_{max} < 2.5$). When the Mullins effect is re-activated, the next loading response exhibits a clear softening. As a consequence, one only needs to compare the difference between two successive loading responses to recognize the Mullins softening activation. The gap between the loading responses of cycle (i) and the previous one (cycle ($i-1$)) may be estimated by various methods. In order to remain consistent with Merckel et al. (2011a), we introduce the parameter α

$$\alpha_{(i)} = \max_{0 \le \sigma \le \max(\sigma_{(i-1)})} \left(\frac{\lambda^{cor}_{(i)}(\sigma)}{\lambda^{cor}_{(i-1)}(\sigma)} \right) \tag{3}$$

quantifying the difference between the stress–stretch responses of two successive cycles. One may notice that α will remain close to 1 as long as the Mullins softening is not activated and α will be different from 1 when the Mullins softening occurs.

Fig. 2b shows the evolution of α according to the maximum stretch applied at each cycle (i) for a virgin sample and for a sample already pre-stretched up to $\lambda_{pre} = 2.5$. For the virgin sample, α is above 1 for each cycle which shows the increase in the material softening. For the pre-stretched sample, α remains close to 1 as long as the sample stretching remains below the maximum pre-stretch, then α evolves suddenly and return onto the α-curve provided by the virgin sample. The parameter α appears as a relevant and obvious indicator of the Mullins activation.

2.3. Results

The softening evolution parameter α defined above is now applied to nonproportional loadings. First, large uniaxial dumbbell samples are submitted to a $\lambda_{pre} = 2.5$ pre-stretch and small dumbbell uniaxial tension samples are punched in the large samples with a direction of 0°, 45° and 90° with respect to the pre-stretch direction. The small specimen are then submitted to cyclic uniaxial tension tests. Fig. 3 presents the parameter α computed on the cyclic uniaxial tension stress–stretch responses according to the angle of cut. One notices the strong dependence of the Mullins softening evolution according to the direction of second loading. As one could expect, for the sample cut along the direction of pre-stretch the Mullins softening re-activates when the material is stretched beyond the pre-stretch, but for the other two samples, cut at 45° and 90° with respect to the pre-stretch direction, the Mullins softening is activated from the very first cycles. It is also

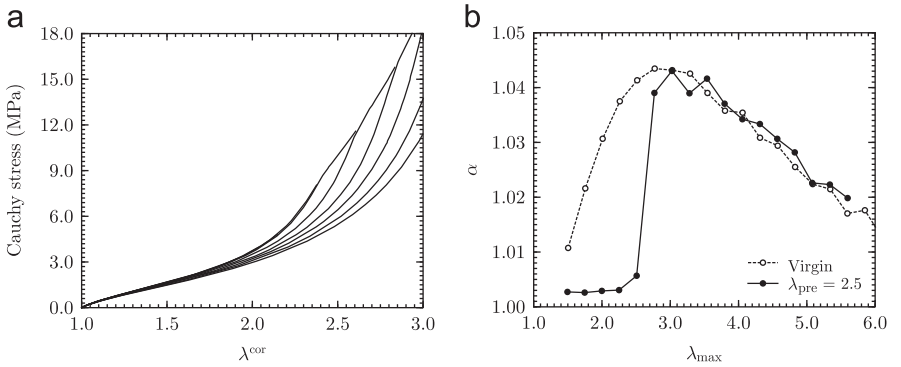

Fig. 2. (a) (λ^{cor},σ) cyclic uniaxial response of samples uniaxially pre-stretched up to $\lambda_{pre} = 2.5$. (b) Parameter α evolution during a cyclic uniaxial tension loading for a virgin sample and for a 2.5-uniaxially pre-stretched sample.

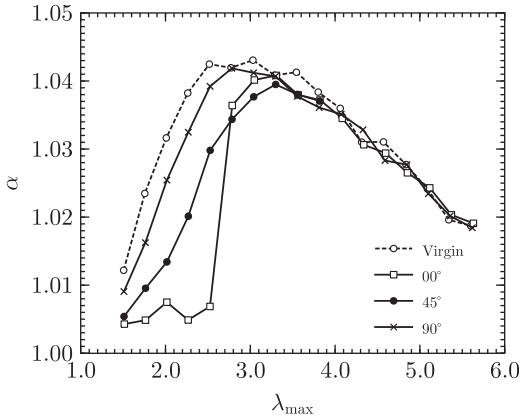

Fig. 3. Parameter α evolution for uniaxially pre-stretched ($F_{11} = 2.5$) samples cut and submitted to a cyclic uniaxial tensions in directions tilted of an angle 0°, 45° or 90° from the direction of pre-stretching.

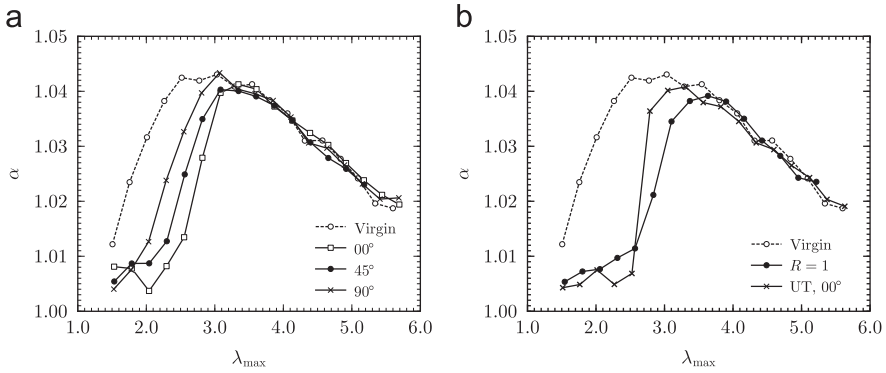

Fig. 4. Parameter α evolution during cyclic uniaxial tension loadings according to the direction of stretching (which compares to the direction of maximum pre-stretch) for biaxially pre-stretched samples up to $F_{11} = 2.5$. (a) $R = 0.5$. (b) Equibiaxial ($R = 1$).

interesting to note that for the sample stretched in the direction of pre-stretching, once the maximum stretch passed the pre-stretch values, the parameter α returns on the evolution of α provided by the virgin sample. For the other samples, during the first cycles, the softening evolves but at a lower rate than for the virgin material, evidencing a softening evolution but from an already pre-damaged state. Finally, the sample cut at 90° and the virgin material show similar softening evolutions.

Biaxial samples were submitted to a biaxial tension preloading defined by $R = 0.5$ and $F_{11} = 2.5$, the resulting stretch in the direction 2 being $F_{22} = 1.75$. Uniaxial dumbbell samples were cut along various directions. Fig. 4a shows the evolutions of α for samples cut in directions displaying angles of 0°, 45° and 90° with respect to the direction 1. These evolutions are progressive for every direction and even though it is not obvious to spot the accurate value of λ_{max} exhibiting Mullins-softening re-activation due to 0.25 stretch steps in between the successive cycles, direction 1 (0°) and direction 2 (90°) Mullins activation stretches seem close to the pre-stretch applied in these directions.

Other biaxial samples were submitted to equi-biaxial tension ($R = 1$) stretching up to $F_{11} = 2.5$. For these samples, it was verified that the cyclic uniaxial tension sample cutting direction had no effect on the softening evolution, the Mullins softening exhibiting in-plane isotropy. Fig. 4b compares the parameter α for a virgin material sample, the uniaxially pre-stretched sample cut along the direction of pre-stretching and the equi-biaxially pre-stretched sample. Both pre-stretch samples show the same threshold of softening activation which corresponds to the pre-stretching. Nonetheless, once this threshold passed, the return of α on the virgin material α-curve is more gradual for the equi-biaxially pre-stretch sample.

These original results are now used to define a three-dimensional Mullins softening criterion.

3. Mullins softening criterion

3.1. Definition

Considering the directional dependence of the Mullins softening activation evidenced in the previous section and its well-known dependence to the maximum stretching, we introduce directional stretching scalars along directions $\boldsymbol{u}$

according to

$$\lambda^{\boldsymbol{u}}(\theta,\varphi,\boldsymbol{C}) = \sqrt{\boldsymbol{u}\cdot\boldsymbol{C}\cdot\boldsymbol{u}} \tag{4}$$

with $\boldsymbol{C}=\boldsymbol{F}^t\boldsymbol{F}$ being the right Cauchy–Green tensor, $\boldsymbol{F}$ being the deformation gradient tensor and $\boldsymbol{u}=(\cos(\theta),\sin(\theta)\cos(\varphi),\sin(\theta)\sin(\varphi))$ unit vectors characterized by their polar angles (θ,φ). We observed that the Mullins softening was evolving when at least one direction was stretched above its maximum stretch already undergone; therefore, we propose the following criterion for the activation of the Mullins softening:

$$\exists \boldsymbol{u}(\theta,\varphi)\,|\,(\lambda^{\boldsymbol{u}}-\lambda^{\boldsymbol{u}}_{\max})=0 \tag{5}$$

with $\lambda^{\boldsymbol{u}}_{\max}$ being the maximum stretch along direction $\boldsymbol{u}$ over the loading history, which writes

$$\lambda^{\boldsymbol{u}}_{\max} = \max_{0\to t}[\lambda^{\boldsymbol{u}}(\boldsymbol{C}(t))]. \tag{6}$$

Let us note that such a Mullins softening activation criterion has been already applied by Diani et al. (2006a,b), Dargazany and Itskov (2009), Merckel et al. (2011b) and studied by Itskov et al. (2010), though without any experimental evidences supporting its relevance.

According to Eq. (6), the Mullins criterion may be represented by the three-dimensional surface defined by $\lambda^{\boldsymbol{u}}_{\max}$. For proportional loadings, one may write analytical expressions specifying the Mullins threshold surface. For nonproportional loadings, the surface contour is reached through numerical computations. Fig. 5 shows the three-dimensional representations of the surfaces resulting from uniaxial, biaxial ($R=0.5$) and equi-biaxial loading conditions, which are the preloading conditions of our study.

The criterion proposed in Eq. (5) is now confronted to the experimental results.

3.2. Analysis

Fig. 6 presents the evolution $\lambda^{\boldsymbol{u}}_{\max}$ with the applied loading for $\lambda_{\text{pre}}=2.5$ uniaxially pre-stretched samples cut in directions 0°, 45° and 90° and submitted to a cyclic uniaxial tension with the maximum stretch increasing of $\Delta\lambda=0.25$ at each cycle. This figure corresponds to the evolution of $\lambda^{\boldsymbol{u}}_{\max}$ for the Mullins softening progression experimentally studied in Fig. 3. In order to ease the understanding, the evolution of $\lambda^{\boldsymbol{u}}_{\max}$ is plotted in the specimen stretching plane. The dashed line draws the preloading surface, the solid lines result from the post uniaxial tension cycles when increasing the dimension of the $\lambda^{\boldsymbol{u}}_{\max}$ surface.

Fig. 6a, corresponding to proportional uniaxial tension loadings, shows that the surface defined by $\lambda^{\boldsymbol{u}}_{\max}$ evolves when the applied stretch goes beyond the initial pre-stretch. Moreover, when evolving, a substantial number of directions are

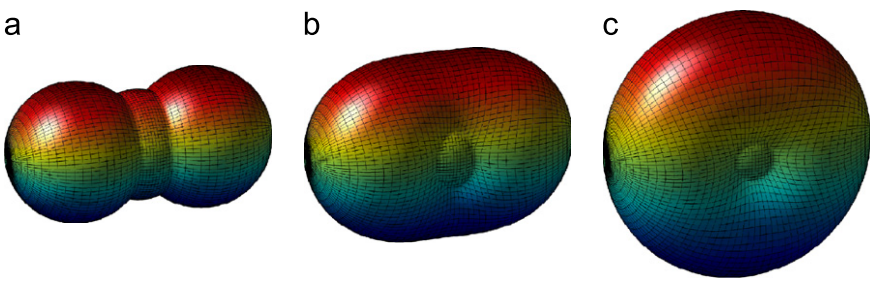

Fig. 5. Three-dimensional representation of the surface defined by $\lambda^{\boldsymbol{u}}_{\max}(\theta,\varphi)$ for a $F_{11}=2.5$ loading in (a) uniaxial tension, (b) $R=0.5$ biaxial tension, and (c) equi-biaxial tension ($R=1$).

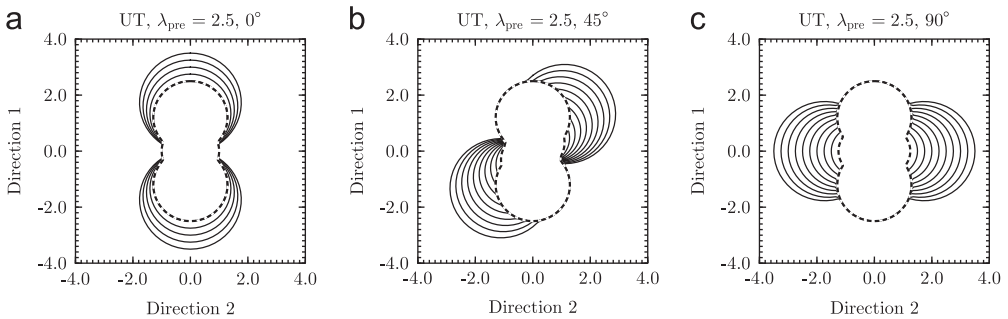

Fig. 6. Projection of the $\lambda^{\boldsymbol{u}}_{\max}(\theta,\varphi)$ surface in the sample plane. Dashed line: uniaxial pre-stretch up to $\lambda_{\text{pre}}=2.5$. Solid line: surface evolution during cyclic uniaxial loadings performed in directions (a) 0°, (b) 45° and (c) 90° compared to the direction of pre-stretching.

affected. For samples cut at 45° (Fig. 6b), the maximum stretching surface evolves from the first cycle and the number of directions affected starts low and grows gradually at each cycle. Fig. 6c shows that the $\lambda^{\boldsymbol{u}}_{\max}$ surface, corresponding to samples cut at 90° with respect to the pre-stretching direction, evolves from the very first cycle.

Fig. 7 shows the evolution of $\lambda^{\boldsymbol{u}}_{\max}$ for a biaxial preloading characterized by $R=0.5$ and $F_{11}=2.5$, followed by a cyclic uniaxial tension at 0°, 45° and 90° with respect to direction 1. This figure compares with Fig. 4a. For this preloading, one may notice that the $\lambda^{\boldsymbol{u}}_{\max}$ surfaces evolve only after reaching a stretch threshold depending on the direction of cut (0°, 45° or 90°), the surfaces evolve after cycles 6, 4 and 3, respectively (corresponding to $\lambda_{\max}$ equal to 2.5, 2 and 1.75, respectively), which corroborates the Mullins softening activation thresholds given by Fig. 4a. A similar $\lambda^{\boldsymbol{u}}_{\max}$ surface analysis works well for the equi-biaxial preloading case also.

The former qualitative analysis may be reinforced by a quantitative analysis of the surface created at each cycle. For this purpose, we introduce the parameter

$$\gamma = \frac{1}{4\pi}\iint_{\mathcal{S}} \gamma^{\boldsymbol{u}} \sin(\theta)\, \mathrm{d}\varphi\, \mathrm{d}\theta \tag{7}$$

with $\gamma^{\boldsymbol{u}}(\theta,\varphi)=1$ when $\partial\lambda^{\boldsymbol{u}}_{\max}/\partial t>0$ and $\gamma^{\boldsymbol{u}}(\theta,\varphi)=0$ when $\partial\lambda^{\boldsymbol{u}}_{\max}/\partial t=0$, t being the time.

Parameter γ, inspired by the former work by Diani and Gilormini (2005), computes the fraction of directions stretched above their maximum stretch already undergone. Fig. 8 shows the values of γ continuously computed for $\lambda_{\max}$ ranging from 1 to 5, for the loading histories studied in Section 2.3. We marked by symbols each cycle of the actual cyclic uniaxial tension tests. This figure is to be compared with Figs. 3 and 4. These figures reveal a strong correlation between α and γ characterizing the increase in material softening and the increase in the $\lambda^{\boldsymbol{u}}_{\max}$ surface, respectively, and they provide solid evidences supporting the relevance of criterion equation (5).

3.3. Validation

We presented a number of experimental results leading to the definition equation (5) of a Mullins softening criterion. The criterion is now tested on other loading conditions. For this purpose, biaxial samples were submitted to different loading histories leading to the same $\lambda^{\boldsymbol{u}}_{\max}$ surfaces. Then uniaxial tension samples were cut at 0°, 45° and 90° and submitted to cyclic uniaxial tension tests. During the latter tests, the Mullins softening activation was estimated with the parameter α and compared according to the loading history.

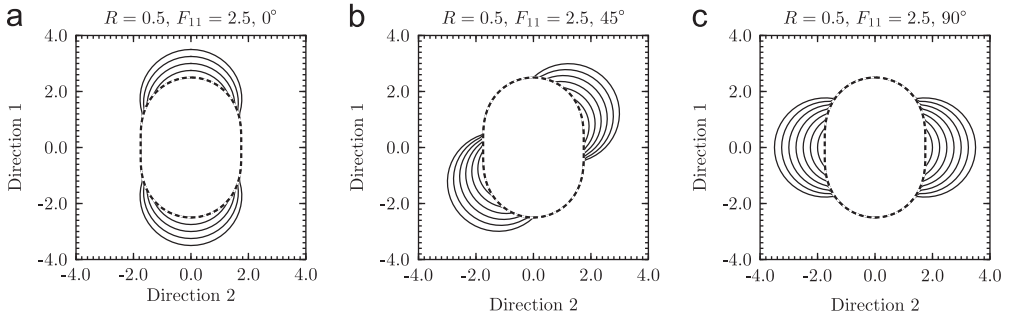

Fig. 7. Projection of the $\lambda^{\boldsymbol{u}}_{\max}(\theta,\varphi)$ surface in the sample plane. Dashed line: $R=0.5$ biaxial pre-stretch up to $F_{11}=2.5$. Solid line: surface evolution during cyclic uniaxial loadings performed in directions (a) 0°, (b) 45° and (c) 90° compared to the direction of pre-stretching.

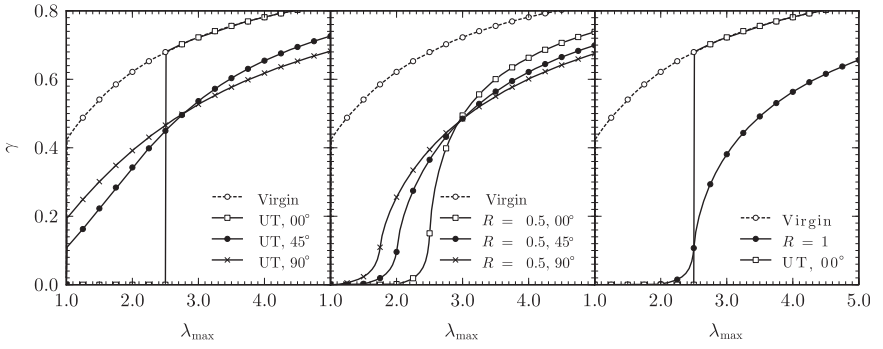

Fig. 8. Fraction of active elongated chains γ evolution during cyclic uniaxial loadings performed in different directions for pre-stretch samples with a $F_{11}=2.5$ loading intensity, preloading paths are grouped according to Figs. 3 and 4.

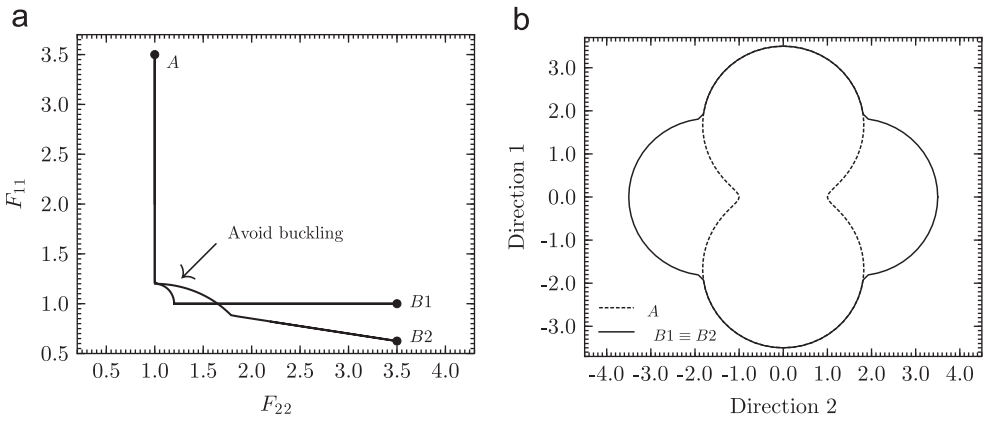

Fig. 9. (a) $F_{11}-F_{22}$ plane schematic representation of two specific loading paths: A to $B1$ and A to $B2$. (b) Projection of $\lambda^{\mathbf{u}}_{\max}(\theta,\varphi)$ surfaces for both loading paths.

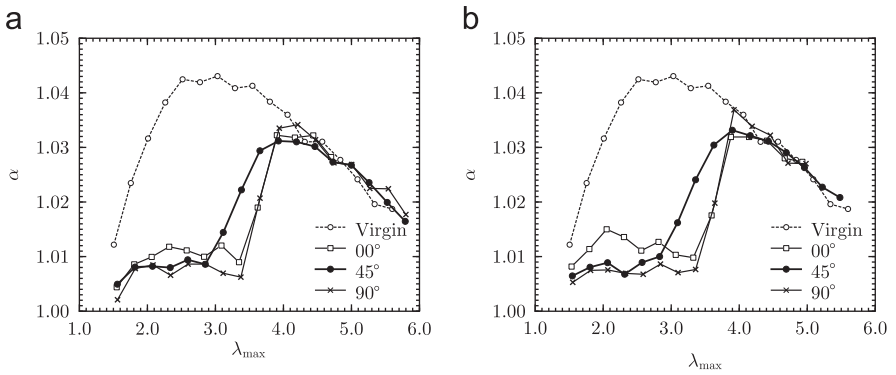

Fig. 10. Parameter α evolution during cyclic uniaxial loadings for (a) path A to $B1$ and (b) path A to $B2$ preloaded samples.

The two loading histories are sketched in Fig. 9a. The first one from A to $B1$ is made of two successive perpendicular pure shear loadings. The second loading from A to $B2$ adds a biaxial compression-tension to the pure shear according to direction 1 (A). Both loading paths cause the identical maximum stretch surface drawn in Fig. 9b and should evolve when uniaxial tension stretches reach $\lambda_{\max}=3.5$, 2.6 and 3.5 according to directions 0°, 45° and 90°, respectively. These paths were chosen specifically for several reasons. First, the resulting maximum stretch surface exhibit an interesting change of convexity at 45°, second, during preloading from A to $B2$, direction 1 is first stretched and then quite severely compressed ($F_{11}=0.62$), which puts to test the criterion when some directions are stretched and then compressed.

Fig. 10 shows the parameter α resulting from the cyclic uniaxial tension stress–stretch responses for samples cut at 0°, 45° and 90° for both preloading cases. One notices that both preloadings lead to the same evolution of the softening parameter α; therefore, both preloadings are identical in terms of Mullins softening. Finally, Fig. 10 shows that Mullins softening activates earlier for samples cut at 45° compare to samples cut in directions 1 and 2 and Fig. 10b illustrates that the post-stretching compression in the direction 1 does not change the evolution of α which is similar for both directions 1 and 2. Therefore, a stretched direction does not recover from its Mullins softening when submitted to a compression. Both results reinforce the well-grounded of criterion equation (5).

4. Conclusion

This contribution aimed at defining a Mullins softening activation criterion for filled rubbers submitted to general loading conditions, including nonproportional loadings. The criterion is grounded on an original analysis of unconventional experimental data. By comparing the stress–stretch responses of successive uniaxial tension cycles with increasing maximum stretch, a softening evolution parameter is defined. According to this softening parameter evolution, it is possible to recognize the Mullins softening activation. The method applies for preloaded samples, and allows the definition of the directional stretch necessary to re-activate the Mullins softening in the direction of cyclic uniaxial stretching. The method has been applied to several samples uniaxially or biaxially preloaded, including proportional and nonproportional post cyclic uniaxial loadings. Results provide solid evidences for the definition of a Mullins softening activation criterion as the three-dimensional surface of maximum directional stretch submitted to the material along the loading history. Also,

two specific loading cases involving different loading paths with identical maximum direction stretch surfaces were considered in order to test the criterion predictive ability. The Mullins softening activation threshold was well predicted by the criterion. The definition of such a valid experimentally based criterion is a critical point for constitutive modeling of the Mullins softening, it should open new perspectives in terms of mechanical modeling.

Acknowledgments

This work was supported by the French "Agence Nationale de la Recherche" through project AMUFISE (MATETPRO 08-320101). The authors acknowledge useful discussions with D. Berghezan, G. Besnard, C. Creton, J. de Crevoisier, F. Hild, C. Moriceau, M. Portigliatti, S. Roux, F. Vion-Loisel, and H. Zhang.

References

Chagnon, G., Verron, E., Gornet, L., Marckmann, G., Charrier, P., 2004. On the relevance of continuum damage mechanics as applied to the Mullins effect in elastomers. J. Mech. Phys. Solids 52 (7), 1627–1650.

Dargazany, R., Itskov, M., 2009. A network evolution model for the anisotropic Mullins effect in carbon black filled rubbers. Int. J. Solids Struct. 46 (16), 2967–2977.

Diani, J., Brieu, M., Gilormini, P., 2006a. Observation and modeling of the anisotropic visco-hyperelastic behavior of a rubberlike material. Int. J. Solids Struct. 43 (10), 3044–3056.

Diani, J., Brieu, M., Vacherand, M., 2006b. A damage directional constitutive model for Mullins effect with permanent set and induced anisotropy. Eur. J. Mech. A Solids 25, 483–496.

Diani, J., Fayolle, B., Gilormini, P., 2009. A review on the Mullins effect. Eur. Polym. J. 45, 601–612.

Diani, J., Gilormini, P., 2005. Combining the logarithmic strain and the full-network model for a better understanding of the hyperelastic behavior of rubber-like materials. J. Mech. Phys. Solids 53 (11), 2579–2596.

Elías-Zúñiga, A., 2005. A phenomenological energy-based model to characterize stress-softening effect in elastomers. Polymer 46 (10), 3496–3506.

Göktepe, S., Miehe, C., 2005. A micro–macro approach to rubber-like materials. Part 3: The micro-sphere model of anisotropic Mullins-type damage. J. Mech. Phys. Solids 53 (10), 2259–2283.

Govindjee, S., Simo, J., 1991. A micro-mechanically based continuum damage model for carbon black-filled rubbers incorporating Mullins' effect. J. Mech. Phys. Solids 39, 87–112.

Govindjee, S., Simo, J., 1992. Transition from micro-mechanics to computationally efficient phenomenology: carbon black filled rubbers incorporating Mullins'effect. J. Mech. Phys. Solids 40, 213–233.

Hanson, D.E., Hawley, M., Houlton, R., Chitanvis, K., Rae, P., Orler, B.E., Wrobleski, D.A., 2005. Stress softening experiments in silica-filled polydimethylsiloxane provide insight into a mechanism for the Mullins effect. Polymer 46 (24), 10989–10995.

Itskov, M., Ehret, R., Weinhold, G., 2010. A thermodynamically consistent phenomenological model of the anisotropic Mullins effect. Z. Angew. Math. Mech. 90 (5), 370–386.

Itskov, M., Halberstroh, E., Ehret, A.E., Vöhringer, M.C., 2006. Experimental observation of the deformation induced anisotropy of the Mullins effect in rubber. Kautsch. Gummi Kunstst. 5555, 93–96.

Krishnaswamy, S., Beatty, M.F., 2000. The Mullins effect in compressible solids. Int. J. Eng. Sci. 38, 1397–1414.

Laraba-Abbes, F., Ienny, P., Piques, R., 2003. A new 'Tailor-made' methodology for the mechanical behaviour analysis of rubber-like materials: 2. Application to the hyperelastic behaviour characterization of a carbon-black filled natural rubber vulcanizate. Polymer 44 (3), 821–840.

Lion, A., 1996. A constitutive model for carbon black filled rubber: experimental investigations and mathematical representation. Continuum Mech. Thermodyn. 8, 153–169.

Machado, G., 2011. Contribution à l'étude de l'anisotropie induite par l'effet Mullins dans les élastomères silicone chargés. Ph.D. Thesis, Université de Grenoble.

Merckel, Y., Diani, J., Brieu, M., Caillard, J., 2011a. Characterization of the Mullins effect of carbon-black filled rubbers. Rubber Chem. Technol. 84 (3), 5555.

Merckel, Y., Diani, J., Roux, S., Brieu, M., 2011b. A simple framework for full-network hyperelasticity and anisotropic damage. J. Mech. Phys. Solids 59, 75–88.

Mullins, L., 1947. Effect of stretching on the properties of rubber. J. Rubber Res. 16 (12), 275–289.

Mullins, L., 1949. Permanent set in vulcanized rubber. India Rubber World 120, 63–66.

Mullins, L., 1950. Thixotropic behavior of carbon black in rubber. J. Phys. Colloid Chem. 54 (2), 239–251.

Mullins, L., 1969. Softening of rubber by deformation. Rubber Chem. Technol. 42, 339–362.

Ogden, R.W., Roxburgh, D.G., 1999. A pseudo-elastic model for the Mullins effect in filled rubber. Proc. R. Soc. London, 2861–2877.

Simo, J.C., 1987. On a fully three-dimensional finite-strain viscoelastic damage model: formulation and computational aspects. Comput. Methods Appl. Mech. Eng. 60, 153–173.